TU Delft

Delft University of Technology

Simultaneous position and displacement sensing using two fibre Bragg grating sensors

Nazeer, Nakash; Groves, Roger M.; Benedictus, Rinze

DOI
10.1117/12.2513415

Publication date
2019

Document Version
Final published version

Published in
Sensors and Smart Structures Technologies for Civil, Mechanical, and Aerospace Systems 2019

Citation (APA)
Nazeer, N., Groves, R. M., & Benedictus, R. (2019). Simultaneous position and displacement sensing using two fibre Bragg grating sensors. In J. P. Lynch, H. Sohn, K.-W. Wang, & H. Huang (Eds.), *Sensors and Smart Structures Technologies for Civil, Mechanical, and Aerospace Systems 2019* (Vol. 10970). Article 109701Z (SENSORS AND SMART STRUCTURES TECHNOLOGIES FOR CIVIL, MECHANICAL, AND AEROSPACE SYSTEMS 2019). SPIE. https://doi.org/10.1117/12.2513415

Important note
To cite this publication, please use the final published version (if applicable).
Please check the document version above.

Copyright
Other than for strictly personal use, it is not permitted to download, forward or distribute the text or part of it, without the consent of the author(s) and/or copyright holder(s), unless the work is under an open content license such as Creative Commons.

Takedown policy
Please contact us and provide details if you believe this document breaches copyrights.
We will remove access to the work immediately and investigate your claim.

This work is downloaded from Delft University of Technology.
For technical reasons the number of authors shown on this cover page is limited to a maximum of 10.

PROCEEDINGS OF SPIE

SPIEDigitalLibrary.org/conference-proceedings-of-spie

Simultaneous position and displacement sensing using two fibre Bragg grating sensors

Nakash Nazeer, Roger M. Groves, Rinze Benedictus

Nakash Nazeer, Roger M. Groves, Rinze Benedictus, "Simultaneous position and displacement sensing using two fibre Bragg grating sensors," Proc. SPIE 10970, Sensors and Smart Structures Technologies for Civil, Mechanical, and Aerospace Systems 2019, 109701Z (27 March 2019); doi: 10.1117/12.2513415

SPIE.

Event: SPIE Smart Structures + Nondestructive Evaluation, 2019, Denver, Colorado, United States

Downloaded From: https://www.spiedigitallibrary.org/conference-proceedings-of-spie on 16 Jul 2019 Terms of Use: https://www.spiedigitallibrary.org/terms-of-use

Simultaneous position and displacement sensing using two fibre Bragg grating sensors

Nakash Nazeer[a], Roger M. Groves[a] and Rinze Benedictus[b]

[a]Aerospace NDT Laboratory, Faculty of Aerospace Engineering, Delft University of Technology, Kluyverweg 1, 2629 HS Delft, The Netherlands;
[b]Structural Integrity & Composites, Faculty of Aerospace Engineering, Delft University of Technology, Kluyverweg 1, 2629 HS Delft, The Netherlands

ABSTRACT

Over the years, many shape sensing methods have been developed with technologies including optical fibre, PZT and fringe projection. Among them, optical fibres have gained a lot of attention due to their unobtrusive nature when either surface mounted or embedded in the structure. Optical fibre Bragg gratings (FBG) are currently employed for structural health monitoring in civil and aerospace systems and their shape sensing capabilities have been previously reported. In this paper, we propose a novel fibre optic based shape sensor of an isotropic cantilever beam based on the principles of interferometry and FBG sensing. The method described in this paper uses a standard single core single-mode optical fibre and the least number of sensors to estimate the shape, making it comparatively an inexpensive sensing method. On displacing the beam with an unknown magnitude and at an unknown location along the beam, we are able to demonstrate that we can measure the shape of the displaced beam and the magnitude and location of the force applied. The analysis involves using a calibration method and an iterative calculation to measure the two unknowns. An analytical model based on the known beam theories was used to assess the accuracy of the measurements. The preliminary analysis yielded an accuracy of ± 1 mm and ± 50 mm for the displacement and location, respectively.

Keywords: Fibre Bragg grating, Strain measurement, Optical interferometry, Shape sensing, Structural health monitoring

1. INTRODUCTION

Shape sensors have been widely used in various fields ranging from civil[1] and aerospace[2] to medical applications.[3] Several methods for shape sensing have been reported over the years. Optical fibre sensors have been used to measure deflection as well as for reconstruction of the shape.[4] Deformation or shape sensing has also been demonstrated using piezoelectric sensors[5] where a network of piezos form a sensing film. Each piezo point acts as an individual sensor that provides local information of the deformation. Another shape sensing method is by projecting light on to the structure where image data is processed using colour coded sensors and by using 'artificial vision' to obtain shape of the object.[6,7] Excluding optical fibres, the above mentioned technologies generally involve a complex mechanism and processing of large amounts of data. Moreover, they are not suitable in environments with harsh conditions or those that are difficult to access. In this regard, optical fibres stand out due to their desirable properties including EMI immunity, corrosion resistance, high sensitivity and compact size.[8]

Among optical fibre methods, deformation shape estimation using modal analysis with the help of fibre Bragg grating sensors have been demonstrated. This technique implements the use of grating sensors to estimate the corresponding displacement field.[9] Recently, strain sensing using dense networks of fibre Bragg grating (FBG) sensors have gained a lot of attention for measurement and estimation of the shape of aircraft wings and turbine blades.[10–12] Combined measurement of the bending strain and vibration of a cantilever beam was also demonstrated using FBG sensors.[13]

Further author information
N.Nazeer@tudelft.nl, R.M.Groves@tudelft.nl, R.Benedictus@tudelft.nl

Sensors and Smart Structures Technologies for Civil, Mechanical, and Aerospace Systems 2019, edited by Jerome P. Lynch, Haiying Huang, Hoon Sohn, Kon-Well Wang, Proc. of SPIE Vol. 10970, 109701Z
© 2019 SPIE · CCC code: 0277-786X/19/$18 · doi: 10.1117/12.2513415

Downloaded From: https://www.spiedigitallibrary.org/conference-proceedings-of-spie on 16 Jul 2019
Terms of Use: https://www.spiedigitallibrary.org/terms-of-use

OFDR has also been used to determine deformation of a structure in three dimensions where self referenced fibres were developed that made use of helically wound multiple cores.[14] The shape is estimated by measuring the axial twist and curvature along the fibre. This technique tends to have higher acquisition periods and is more suitable for static tests[15] rather than dynamic real-time measurements that we are interested in.

To summarise, current fibre optic shape sensing methods typically incorporate grating sensors[10,11,16,17] in rather complex configurations containing either multiple cores[18,19] or a single core with distributed gratings.[20,21] These methods typically involve Bragg gratings arranged along multiple fibres or cores corresponding to spatial coordinates of the strain sensors. Different geometrical configurations containing these sensors can be designed based on application. The limiting point though, is that these fibre sensors tend to be costly.[22] They require complicated sensor fabrication techniques or multiple sensors that increase the overall cost of the sensor.

In this study, our aim was to develop a simple sensing method that does not require complex and intricate manufacturing procedures and was comparatively inexpensive. For preliminary studies, our focus was on 1-dimensional bend sensing to confirm the working principle of the proposed method. In this paper we demonstrate that with just two FBGs, forming an arrangement similar to a long Fabry-Pérot configuration, values of both the position and displacement of a cantilever beam can be determined.

The paper is organized as follows. Section 2 explains the theories on which this method is based. Section 3 introduces the principle of the approach and describes the experimental design including the setup, the calibration steps and the measurements and is followed by the results in section 4. Section 5 discusses the findings and finally, section 6 concludes the paper.

2. THEORY

This work makes use of the principles of fibre Bragg gratings and of intrinsic Fabry-Pérot interferometers.

A fibre Bragg grating is a segment in an optical fibre that consists of a periodic modulation of the core refractive index. When incident light illuminates the grating, part of it is reflected whereas the rest gets transmitted. On interacting with the refractive index perturbations, a narrowband of the incident optical field, by successive coherent scattering from the index variation, is reflected with a central wavelength. This wavelength is referred to as the Bragg wavelength[23] and is given by:

$$\lambda_B = 2n_{eff}\Lambda \tag{1}$$

Where λ_B is the Bragg wavelength, n_{eff} is the refractive index of the core, and Λ is the periodic spacing of the grating.

The Bragg wavelength (λ_B) shifts when the gratings are subjected to external (mechanical or thermal) disturbances. This shift in wavelength is denoted by $\Delta\lambda_{BS}$. The strain can be expressed as a shift in this Bragg wavelength as:[22]

$$\Delta\varepsilon = \frac{\Delta\lambda_{BS}}{(1-\rho_a)\lambda_B} \tag{2}$$

Where $\Delta\varepsilon$ is the change in strain and ρ_a is the photoelastic coefficient ≈ 0.22.

In the Fabry-Pérot interferometer, the two gratings form what we consider a long Fabry-Pérot cavity.[22] A Fabry-Pérot cavity essentially consists of an optically transparent medium with parallel reflectors (gratings in this case) on either sides. The basic principle is based on the multiple wave interferences. The Free Spectral Range gives the frequency spacing of its transmission peaks within the cavity. This FSR divided by the bandwidth (FWHM) is referred to as the finesse of the cavity. Generally, narrower finesses are preferred. The cavity length between the two gratings can be determined by wavelength scanning and is changed in the presence of an external disturbance. This change in length is related to the strain by:

Downloaded From: https://www.spiedigitallibrary.org/conference-proceedings-of-spie on 16 Jul 2019
Terms of Use: https://www.spiedigitallibrary.org/terms-of-use

$$\varepsilon = \frac{\Delta d}{L} \tag{3}$$

Where d is the change in cavity length and L (denoted as L_sensor in the following sections) is the effective sensing length between the two gratings.

3. METHODOLOGY

3.1 Principle

A schematic of the experiment along with the coordinate system and nomenclature used is defined in Figure 1. The optical fibre is fixed to an aluminium beam, aligned along the x axis, with length L, breadth b, and thickness h. A force (F) is applied in the negative y axis. This force causes a displacement in the negative y direction which varies along the beam length.

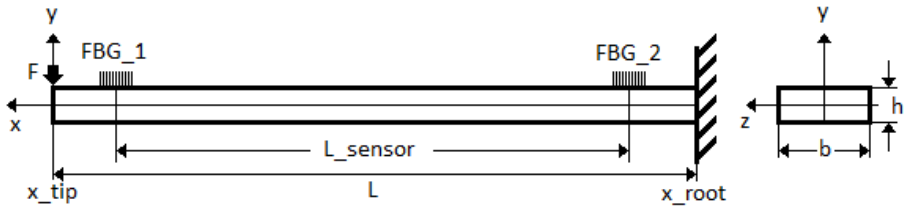

Figure 1: Diagram and definition of the coordinate system of the setup. The beam has length L, breadth b, and thickness h. The position of the two FBGs are shown along with the effective sensor length, L_sensor.

Assuming the deflection applied at $x = x\_tip$ is δ, the strain at that point can be determined using:[13]

$$\varepsilon(x) = \frac{3h\delta x}{2L^3} \tag{4}$$

Where x is any point along the length of the beam measured from x_root.

3.2 Experimental setup

The beam under consideration was aluminium of length $L = 1.05$ m, breadth $b = 0.025$ m and height $h = 0.0015$ m. The beam was mounted in a setup horizontal to the optical table. To form a cantilever, the beam was firmly clamped at one end whilst the other was left free. These ends will further be referred to as the root and tip, respectively. A standard single mode 2 FBG array fibre was bonded on one side of the beam along its length. The nominal Bragg wavelength of FBG_2 and FBG_1 are 1540.258 nm and 1529.901 nm, respectively. The gratings are both 3 mm long with reflectivity levels above 80%. The positions of the gratings FBG_2 and FBG_1 on the cantilever beam are at approximately $x = 0.025$ m and $x = 1.025$ m, respectively, from the root. The length between the two gratings (L_sensor) formed the effective sensing zone.

Experimental values of equation 4 were measured from the setup shown in Figure 2. A linear actuator (Zaber NA23C60-T4) and controller stage allowing a deflection range of 0 to 60 mm were affixed onto a base plate mounted on a slider. The actuator provided deflections at $x = x\_tip$ which was 1.05 m from the root. The deflections were applied at the tip and mid point of the beam individually at steps of 4, from 0 to 20 mm. The optical system (Optics11 ZonaSens) measured the displacement (L m) between the two gratings for each deflection step. A second measurement system, an FBG interrogator, (National Instruments, PXIe-4844) measured the local strain at the root using the grating FBG_2.

Downloaded From: https://www.spiedigitallibrary.org/conference-proceedings-of-spie on 16 Jul 2019
Terms of Use: https://www.spiedigitallibrary.org/terms-of-use

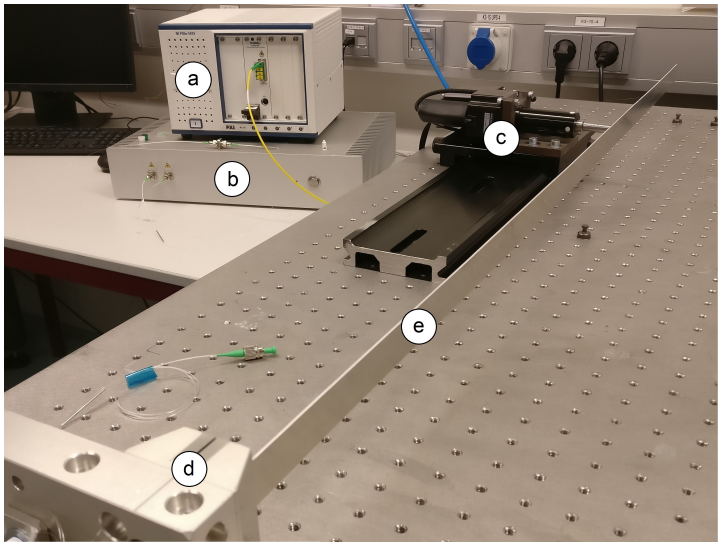

Figure 2: The experimental setup containing the (a) Optics11 interrogator, (b) National Instruments interrogator, (c) linear displacement stage actuator, (d) clamp end and the (e) beam is displayed. The beam with the optical fibre containing the two FBGs running along its length is clamped at one end to form a cantilever.

3.2.1 Calibration

In order to calibrate the setup and record baseline data two sets of measurements were carried out at the tip and mid point of the beam.

Firstly, the actuator stage was set to apply deflections at the tip of the beam (L $\approx$ 1.025 m) in the range 0 to 20 mm in 4 mm steps. Table 1a and Figure 3a display the values recorded along with a comparison with the analytical model.

Following the same setup and procedure as the previous experiment, the deflections were applied at the middle of the beam (L $\approx$ 0.525 m) in the range 0 to 20 mm in 4 mm steps. Table 1b and figure 3b compare the recordings with the analytical model for this case.

The data recorded from the calibration measurements were later used for finding the location and magnitude of an unknown load.

Downloaded From: https://www.spiedigitallibrary.org/conference-proceedings-of-spie on 16 Jul 2019
Terms of Use: https://www.spiedigitallibrary.org/terms-of-use

Table 1: Comparison between the analytical values calculated from equation 4 and experimental values of ΔL in μm for deflections applied at the a) Tip of the beam (L ≈ 1.025 m) and b) Mid point of the beam (L ≈ 0.525 m). The deflections are in steps of 4 from 0 mm to 20 mm.

(a)

Deflection (mm)	**Analytical ΔL (μm)**	**Experimental ΔL (μm)**
0	0	0
4	4.28	5.1
8	8.57	10.3
12	12.8	15.6
16	17.1	21.3
20	21.4	26.8

(b)

Deflection (mm)	**Analytical ΔL (μm)**	**Experimental ΔL (μm)**
0	0	0
4	8.57	9.7
8	17.1	19.8
12	25.7	30.2
16	34.2	40.7
20	42.8	50.1

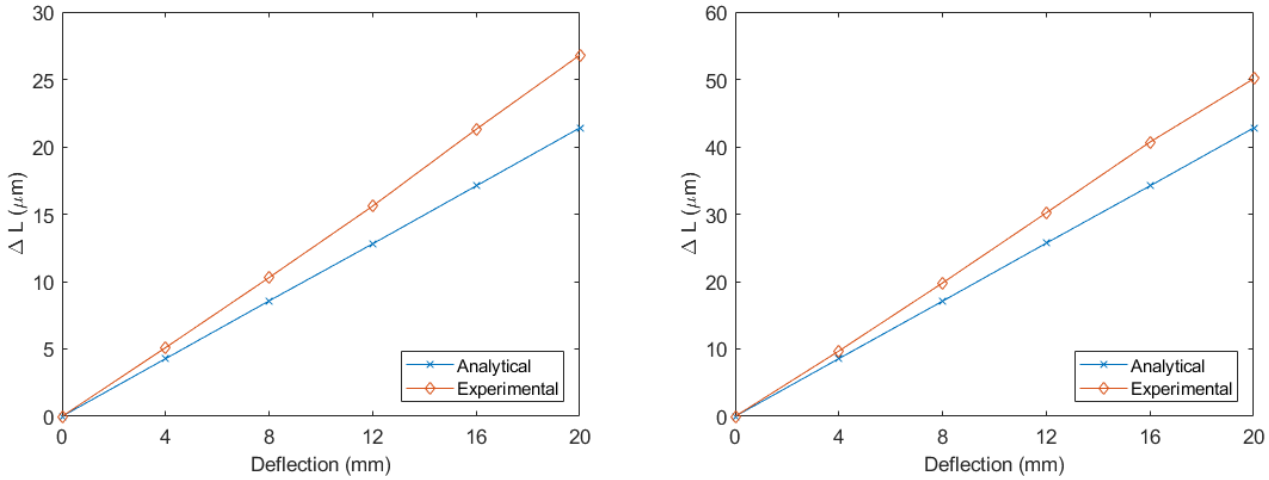

(a) (b)

Figure 3: Graphical representation of the displacement ΔL with respect to deflection for load applied at the a) Tip of the beam, b) Mid point of the beam.

Downloaded From: https://www.spiedigitallibrary.org/conference-proceedings-of-spie on 16 Jul 2019
Terms of Use: https://www.spiedigitallibrary.org/terms-of-use

3.3 Deflection at an unknown location and unknown deflection

The next step is to be able to determine the location of an unknown deflection at an unknown location along the beam. For this, along with the displacement (ΔL) measurements, local strain measurements (ε) were recorded by the FBG_2 at the point x_root. For each displacement step, the corresponding change in length and FBG_2 strain values are tabulated in table 2 and table 3 for tip and mid point load cases, respectively.

Table 2: Values of displacement (ΔL) and strain (ε) measured between the FBGs and at FBG_2, respectively, for deflections applied at the tip of the beam (L $\approx$ 1.025 m). The deflections are in steps of 4 from 0 mm to 20 mm.

Deflection at tip (mm)	ΔL (μm)	ε (μ)
0	0	0
4	5.1	7.49
8	10.3	14.15
12	15.6	21.4
16	21.3	28.29
20	26.8	34.96

Table 3: Values of displacement (ΔL) and strain (ε) measured between the FBGs and at FBG_2, respectively, for deflections applied at the mid point of the beam (L $\approx$ 0.525 m). The deflections are in steps of 4 from 0 mm to 20 mm.

Deflection at mid (mm)	ΔL (μm)	ε (μ)
0	0	0
4	9.7	30.8
8	19.8	55.76
12	30.2	82.39
16	40.7	108.2
20	50.1	135.6

4. RESULTS

Measurements were first carried out for two known positions on the beam which served as baseline reference measurements. The first and second set were taken with deflections applied at the tip and mid point of the beam, respectively. The loading point and displacement measurements were calculated through an iterative computation using the equation:

$$x = \frac{y - y_1}{y_2 - y_1}(x_2 - x_1) + x_1 \tag{5}$$

Where x_1, x_2, y_1 and y_2 are reference measurements (taken from the first calibration step) for a given iteration cycle and x and y are the unknowns. The calculated values are then taken as reference measurements for the next iteration and the cycle continues till the values converge.

Downloaded From: https://www.spiedigitallibrary.org/conference-proceedings-of-spie on 16 Jul 2019
Terms of Use: https://www.spiedigitallibrary.org/terms-of-use

From figures 3a and 3b, although both the experimental and analytical results followed a linear and increasing trend, the former had a different slope. As a consequence, this would have an effect on the accuracy of further calculations. From equation 4 it can be noted that the variables h, x and L play a role in determining the slope of the line. As the experimental measurements only take into account the value of L, the mismatch was identified as due to the inaccuracy in the length. The sensor length (L_sensor) is approximated as 1 m in the middle of the beam with an average clearance of 0.025 m at each end. On the other hand, the analytical model considers the full length of 1.05 m spanning from x_root to x_tip. Additionally, the uncertainty in the grating location increases the variation between the predicted and achieved results. Although the location of the grating is roughly estimated to be within a range specified by the manufacturer, it is difficult to know the exact position of the grating on the fibre hence increasing the uncertainty in the length.

The simultaneous position and deflection sensing is carried out using displacement and strain measurements through two fibre Bragg gratings. The displacement was calculated through the change in length between the two gratings due to applied deflections. The local strain was calculated at the root through the grating FBG_2. Assuming a deflection of unknown magnitude taking place at an unknown location along the beam, the readings from the two gratings was used to approximate the unknown variables by making use of the baseline measurements. This was carried out by a two-step calculation involving a calibration method and an iterative computation. The preliminary calculations without accounting for the errors yielded a good estimate of the unknowns. An accuracy of ± 1 mm and ± 50 mm for magnitude of deflection and the location of applied deflection were achieved, respectively.

5. DISCUSSION

These results show the possibility of monitoring the 1-Dimensional shape of the beam by determining the magnitudes of deflection and location of the displacement along the beam and hence proves the working of the proposed method. Factors including uncertainty in the length of the sensing zone, location of the grating, and beam vibrations where identified as sources of error in the experiment. By further calibrations and accounting for the errors a higher measurement accuracy can be achieved. This study sets the basis for a 2-Dimensional shape sensor that is intended to monitor the bending and torsion of any plate structure. This will also be extended to multiple loading conditions.

6. CONCLUSIONS

The paper presents a novel method to measure the position and displacement of a cantilever beam by using the least number of sensors. The principles of interferometry and fibre Bragg grating were used in combination to acquire data on bending of the beam. This was done with the help of two fibre Bragg gratings along the fibre that form a gap similar to a long Fabry-Pérot cavity. The change in optical distance between the gratings as well as point strain readings were measured. An iterative calculation was performed to converge to the values of the magnitude of deflection being applied and its location along the beam. The results show good approximation (± 1 mm and ± 50 mm for the displacement and location, respectively) with the actual values and the sources of errors were identified. As the results are independent of the properties of the structure in consideration, this approach can be applied to beams of any material.

ACKNOWLEDGEMENTS

This work is part of the strategic project SmartX in the Aerospace Structures and Materials department, Faculty of Aerospace Engineering, Delft University of Technology. The project is focussed on the design and development of smart wing technology.

REFERENCES

1. A. Barrias, J. Casas, and S. Villalba, "A review of distributed optical fiber sensors for civil engineering applications," *Sensors* **16**(5), p. 748, 2016.
2. M. Gherlone, P. Cerracchio, and M. Mattone, "Shape sensing methods: Review and experimental comparison on a wing-shaped plate," *Progress in Aerospace Sciences* **99**, pp. 14 – 26, 2018.

Downloaded From: https://www.spiedigitallibrary.org/conference-proceedings-of-spie on 16 Jul 2019
Terms of Use: https://www.spiedigitallibrary.org/terms-of-use

3. F. Parent, S. Loranger, K. Kanti Mandal, V. Lambin Iezzi, J. Lapointe, J.-S. Boisvert, M. D. Baiad, S. Kadoury, and R. Kashyap, "Enhancement of accuracy in shape sensing of surgical needles using optical frequency domain reflectometry in optical fibers," *Biomedical Optics Express* **8**, pp. 2210–2221, 2017.
4. C. Waltermann, J. Koch, M. Angelmahr, J. Burgmeier, M. Thiel, and W. Schade, "Fiber-optical 3d shape sensing," in *Planar Waveguides and other Confined Geometries: Theory, Technology, Production, and Novel Applications*, G. Marowsky, ed., pp. 227–250, Springer New York, 2015.
5. C. Rendl, D. Kim, S. Fanello, P. Parzer, C. Rhemann, J. Taylor, M. Zirkl, G. Scheipl, T. Rothländer, M. Haller, and S. Izadi, "Flexsense: A transparent self-sensing deformable surface," in *Proceedings of the 27th Annual ACM Symposium on User Interface Software and Technology, UIST '14*, pp. 129–138, ACM, 2014.
6. Z. Zhang, "Review of single-shot 3d shape measurement by phase calculation-based fringe projection techniques," *Optics and Lasers in Engineering* **50**(8), pp. 1097 – 1106, 2012.
7. S. Chen, Y. Li, Q. Guan, and G. Xiao, "Real-time three-dimensional surface measurement by color encoded light projection," *Applied Physics Letters* **89**, pp. 111108 – 111108, 10 2006.
8. E. Udd and W. Spillman, *Fiber Optic Sensors: An Introduction for Engineers and Scientists: Second Edition*, Wiley, 2011.
9. A. Derkevorkian, S. Masri, J. Alvarenga, H. Boussalis, J. Bakalyar, and W. L. Richards, "Strain-based deformation shape-estimation algorithm for control and monitoring applications," *AIAA Journal* **51**, pp. 2231–2240, 09 2013.
10. "Real-time shape sensing to monitor flexible structures," *NASA Dryden Flight Researc center, Edwards, CA,* (Technology Opportunity DRC-006-024), 2010.
11. H.-I. Kim, J.-H. Han, and H.-J. Bang, "Real-time deformed shape estimation of a wind turbine blade using distributed fiber Bragg grating sensors," *Wind Energy* **17**(9), pp. 1455–1467, 2011.
12. H.-I. Kim, L.-H. Kang, and J.-H. Han, "Shape estimation with distributed fiber Bragg grating sensors for rotating structures," *Smart Materials and Structures* **20**(3), p. 035011, 2011.
13. Y. Mizutani and R. M. Groves, "Multi-functional measurement using a single FBG sensor," *Experimental Mechanics* **51**(9), pp. 1489–1498, 2011.
14. E. M. Lally, M. Reaves, E. Horrell, S. Klute, and M. E. Froggatt, "Fiber optic shape sensing for monitoring of flexible structures," *Proc. SPIE Smart Structures and Materials + Nondestructive Evaluation* **8345**, pp. 83452Y – 83452Y–9, 2012.
15. A. Gemes, A. Fernndez-Lpez, and B. Soller, "Optical fiber distributed sensing - physical principles and applications," *Structural Health Monitoring* **9**(3), pp. 233–245, 2010.
16. C.-Y. Lin, L. A. Wang, and G.-W. Chern, "Corrugated long-period fiber gratings as strain, torsion, and bending sensors," *J. Lightwave Technol.* **19**(8), pp. 1159 – 1168, 2001.
17. G. C. Kirby, D. K. Lindner, M. A. Davis, and A. Kersey, "Optimal sensor layout for shape estimation from strain sensors," *SPIE* **2444**, pp. 367 – 376, 1995.
18. G. M. H. Flockhart, W. N. MacPherson, J. S. Barton, J. D. C. Jones, L. Zhang, and I. Bennion, "Two-axis bend measurement with Bragg gratings in multicore optical fiber," *Opt. Lett.* **28**(6), pp. 387–389, 2003.
19. M. Gander, W. Macpherson, R. Mcbride, J. Jones, L. Zhang, I. Bennion, P. Blanchard, J. Burnett, and A. Greenaway, "Bend measurement using Bragg gratings in multicore fibre," *Electronics Letters* **36**, pp. 120 – 121, 2000.
20. M. J. Nicolas, R. W. Sullivan, and W. L. Richards, "Large scale applications using FBG sensors: Determination of in-flight loads and shape of a composite aircraft wing," *Aerospace* **3**(3), pp. 18–1 – 18–15, 2016.
21. C. V. Jutte, W. L. Ko, C. A. Stephens, J. A. Bakalyar, W. L. Richards, and A. R. Parker, "Deformed shape calculation of a full-scale wing using fiber optic strain data from a ground loads test," (NASA/TP2011215975), 2011.
22. A. D. Kersey, "A review of recent developments in fiber optic sensor technology," *Optical Fiber Technology* **2**(3), pp. 291 – 317, 1996.
23. A. D. Kersey, M. A. Davis, H. J. Patrick, M. LeBlanc, K. P. Koo, C. G. Askins, M. A. Putnam, and E. J. Friebele, "Fiber grating sensors," *Journal of Lightwave Technology* **15**(8), pp. 1442–1463, 1997.

Downloaded From: https://www.spiedigitallibrary.org/conference-proceedings-of-spie on 16 Jul 2019
Terms of Use: https://www.spiedigitallibrary.org/terms-of-use